

## ANNIHILATION RADIATION IN THE GALAXY

C. D. Dermer and R. J. Murphy

Code 7650, Naval Research Laboratory, Washington, DC 20375-5352, USA

### ABSTRACT

Observations of annihilation radiation in the Galaxy are briefly reviewed. We summarize astrophysical mechanisms leading to positron production and recent estimates for production rates from nova and supernova nucleosynthesis in the Galaxy. The physical processes involved in the production of annihilation radiation in the interstellar medium are described. These include positron thermalization, charge exchange, radiative recombination, and direct annihilation. Calculations of  $2\gamma$  and  $3\gamma$  spectra and the positronium (Ps) fraction due to the annihilation of positrons in media containing H and He at different temperatures and ionization states are presented. Quenching of Ps by high temperature plasmas or dust could account for differences between 0.511 MeV and  $3\gamma$  Ps continuum maps. These results are presented in the context of the potential of *INTEGRAL* to map sites of annihilation radiation in the Galaxy. Positron production by compact objects is also considered.

Key words: positrons; gamma rays; nucleosynthesis; supernovae.

### 1. INTRODUCTION

With an omnidirectional flux of  $\approx 2.6 \times 10^{-3}$  ph cm $^{-2}$  s $^{-1}$ , the  $e^+e^-$  annihilation line at 0.511 MeV is the brightest gamma-ray line in the Galaxy. Associated with the  $2\gamma$  line is the  $3\gamma$  positronium continuum formed by the decay of Positronium (Ps) atoms in the  $^3S_1$  state. The fraction of positrons that annihilate via the formation of Ps depends on the temperature, density, composition, and dust content of the medium. Consequently observations of  $2\gamma$  and  $3\gamma$  fluxes and line widths reveal the ISM properties at sites where positrons annihilate. Past missions have provided limited information on ISM conditions at localized sites because they employed non-imaging detectors with large fields-of-view (FoVs). Moreover, many earlier annihilation line observations used scintillation detectors rather than germanium spectrometers, and so were not able to resolve the width of the

0.511 MeV line. The capability of *INTEGRAL* to resolve and image the annihilation line — though not without considerable technical hurdles — promises to revolutionize our view of the Galaxy in the light of the  $e^+e^-$  annihilation line.

This review summarizes the status of annihilation line astrophysics in the period following the demise of the *Compton Gamma Ray Observatory* and preceding the launch of *INTEGRAL*. In Section 2, past observations of annihilation radiation in the Galaxy are briefly reviewed. Section 3 summarizes the principal astrophysical processes that yield positrons, including recent calculations of positron production by novae, supernovae, cosmic rays, and galactic compact objects. Physical processes leading to the  $2\gamma$  line and  $3\gamma$  continuum are summarized in Section 4, and new calculations of line and continuum spectra and  $3\gamma/2\gamma$  flux ratios in different media are presented in Section 5. The review is concluded in Section 6 with a discussion of prospects for *INTEGRAL* to identify the origin of positrons that produce annihilation radiation, including positron production by Galactic compact objects.

### 2. SPECTRA OF GALACTIC ANNIHILATION RADIATION

The spectrum of the Galaxy as measured by a soft  $\gamma$ -ray telescope is complicated not only by the internal and particle backgrounds of the detector, but also by variable Galactic  $\gamma$ -ray point sources and the unknown distribution of diffuse emissions in the Galaxy. These technical difficulties have been dealt with in a variety of ways, leading to our present incomplete picture of the annihilation emission of the Galaxy.

The 0.511 MeV line was originally discovered by the Rice University group (Johnson & Haymes, 1973), though positive identification of the line required the flight of a germanium detector (Leventhal et al., 1978) which showed that the line, averaged over the 15° FoV of the Bell-Sandia telescope, has a FWHM width  $\Delta E < 3.2$  keV. Other observations of annihilation radiation have employed broad field-of-view instruments, the largest being the 130° FWHM FoV of the *Solar Maximum Mission Gamma Ray Spectrometer*.

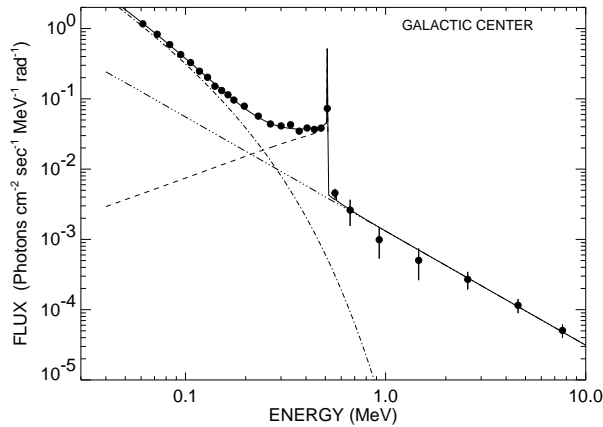


Figure 1. OSSE spectrum of the Galactic Center region during Viewing Periods 5 and 16, showing the 0.511 MeV line and the residual radiation separated into the  $3\gamma$  positronium continuum and background emissions.

eter (Share et al., 1988). By showing that the measured flux correlates with the opening angle of the detector, Lingenfelter & Ramaty (1989) firmly established that there exists a diffuse component of the annihilation radiation in the Galaxy. They also argued for the existence of a variable, time-dependent source of annihilation radiation on the basis of multiple observations made with the HEAO-3 and Bell-Sandia germanium spectrometers. Later analysis of the HEAO-3 data (Mahoney et al., 1994) showed that the evidence for a variable point source was marginal, and no evidence for a variable annihilation component has been obtained through 5.5 (Purcell et al., 1997) and 8.5 (Milne et al., 1999) years of observations of the Galactic Center region with the OSSE instrument on *Compton GRO*.

OSSE has been used to measure the Galactic annihilation radiation in the greatest detail (Milne et al., these proceedings). With a FWHM FoV of  $11.4^\circ \times 3.8^\circ$ , representing about 0.1% of the full sky, OSSE can map annihilation radiation through multiple observations in different directions. This requires offset pointing to subtract background and sophisticated mapping techniques to map diffuse emission. An observation lasting for two 2-week periods is shown in Fig. 1, and illustrates the dominant features in the spectrum of a Galactic Center pointing. Shown is the spectrum measured during Viewing Periods 5 and 16 (Kinzer et al., 1999). The prominent 0.511 MeV annihilation line has a flux of  $\phi_{2\gamma} = 1.8 \pm 0.19 \times 10^{-4}$   $\text{ph cm}^{-2} \text{s}^{-1}$ . The deduced flux of the  $3\gamma$  continuum is  $\phi_{3\gamma} = 10.50 \pm 0.64 \text{, pur97} \times 10^{-4} \text{ ph cm}^{-2} \text{s}^{-1}$ .

The omnidirectional flux of 0.511 MeV annihilation radiation measured with the *Solar Maximum Mission* is  $\phi_{2\gamma} = 23_{-8}^{+5} \times 10^{-4} \text{ ph cm}^{-2} \text{s}^{-1}$ , though the precise flux measurement depends on whether the underlying distribution of the annihilation radiation is assumed to be described by a Galactic Center point source or a distribution described by, for example,

the galactic CO emission (Share et al., 1990; Harris et al., 1990). The omnidirectional flux inferred (Purcell et al., 1997) through analyses of OSSE and earlier annihilation line observations is  $\phi_{2\gamma} = 28 \pm 4 \times 10^{-4} \text{ ph cm}^{-2} \text{s}^{-1}$ , consistent with the *SMM* result.

Naively assuming that the bulk of the annihilation takes place at the distance of the Galactic Center implies a total Galactic annihilation rate of  $\dot{N}_{2\gamma} \approx 4\pi(8 \text{ kpc})^2 \phi_{2\gamma} \approx 2 \times 10^{43} \text{ ph s}^{-1}$ . Letting  $f$  represent the fraction of positrons that annihilate via the intermediate formation of Ps, then each  $e^+$  produced  $2[(1-f) + (f/4)]$  annihilation photons, because a Ps atom decays 1/4 of the time via the  $2\gamma$  state. If  $f \cong 0.9$ , as implied by spectral analyses, then positron sources in the Milky Way are producing a time-averaged rate  $\approx 3 \times 10^{43} \text{ e}^+ \text{s}^{-1}$ .

The structure in the distribution of annihilation radiation can be determined either through model-dependent (Skibo, 1993) or model-independent (Purcell et al., 1997; Cheng et al., 1997; Milne et al., 1999) mapping techniques. In the former approach, one assumes that the annihilation radiation is described by model spatial distributions, for example, those describing novae, pulsars, hot plasma, or  $> 100$  MeV gamma-ray distributions. One then minimizes  $\chi^2$  of the observations with respect to various superpositions of the model distributions. This method is limited if the model distributions provide a poor characterization of features peculiar to the true spatial distribution of annihilation radiation. These methods were used to argue that a disk component, a bulge feature related to an old stellar population, and a time-variable point source were required to fit available 0.511 MeV line observations (Ramaty et al., 1994).

Model-independent mapping techniques, employing Singular Value Decomposition or the Maximum Entropy Method algorithms, can be used to reconstruct the image without recourse to assumptions about underlying model distributions. Using these methods, Purcell et al. (1997) showed that OSSE observations were described by the following emission components:

- Positive galactic plane:  $2.9 \pm 0.2$ ,
- Negative galactic plane:  $3.1 \pm 0.3$ ,
- Central bulge:  $6.0 \pm 0.4$ ,
- Positive latitude enhancement:  $2.2 \pm 0.2$ ,
- Mirror region:  $0.8 \pm 0.1$ ,

where the fluxes are given in units of  $10^{-4} \text{ ph cm}^{-2} \text{s}^{-1}$ . This analysis results in a flux for the full map of  $22.5 \pm 0.7 \text{ ph cm}^{-2} \text{s}^{-1}$ , which is consistent with the omnidirectional flux quoted earlier when consideration of emission in regions not observed with OSSE was included. The asymmetry associated with the positive latitude enhancement has been interpreted

Table 1. Positron production processes and mean production Lorentz factors

| Processes  | $\langle \gamma \rangle$ |
|--|--------------------------|
| $N^* \rightarrow N + e^+$                          | few                      |
| $N + p \rightarrow \pi^+ \rightarrow e^+$          | $\gtrsim 60$             |
| $N + N' \rightarrow N^* \rightarrow N + e^+$       | $\gtrsim$ few            |
| $e + B \rightarrow \gamma + B \rightarrow e^+ e^-$ | $\sim 10^6$ - $10^8$     |
| $\gamma\gamma \rightarrow e^+ e^-$                 | $\gtrsim$ few            |

(Dermer & Skibo, 1997) in terms of annihilation fountain of pair-laden hot plasma driven by a starburst from the Galactic Center region into the halo of the Galaxy.

Later analysis (Milne et al., 1999) has confirmed that the positive latitude enhancement has a flux  $\phi_\gamma \cong 1$ - $2 \times 10^{-4}$  ph cm $^{-2}$  s $^{-1}$ , though there is only marginal evidence for a high-latitude enhancement in the  $3\gamma$  positronium map. This implies that Ps is quenched in the fountain, either because the temperature is very high or the region is dusty. The first possibility can be determined by measuring the line width of the annihilation radiation in this direction, and will be discussed in more detail in the Section 5.

### 3. POSITRON PROCESSES AND PRODUCTION SITES

As we have seen, sources must produce  $\approx 3 \times 10^{43}$  e $^+$  s $^{-1}$  to account for the diffuse annihilation glow of the Milky Way. Table 1 lists astrophysical processes that make positrons. The first row represents channels where e $^+$  are produced through  $\beta^+$  decay of nuclei formed in explosive and hydrostatic nucleosynthesis of novae, supernovae (SNe), Wolf-Rayet and Asymptotic Giant Branch stars. The positrons produced through this channel have a characteristic  $\beta^+$  decay spectrum with typical kinetic energies of  $\sim 1$  MeV. The second row represents secondary production interactions between cosmic ray protons and ions that produce a characteristic  $\pi^+$  decay spectrum of positrons peaking at  $\sim 30$  MeV. Positrons can also be produced in stellar flares through this process. The third row represents cosmic ray interactions that form ions which subsequently decay through the emission of positrons. Depending on whether the ions are at rest or are in motion, positrons are formed with Lorentz factors ranging from only a few to values roughly equal to the Lorentz factors of the excited ion. This process can be important in stellar flares and in accreting neutron stars and black holes, and in regions with enhanced fluxes of low-energy cosmic rays.

The fourth row represents positrons formed by pulsar electromagnetic cascades. Here curvature or synchrotron photons materialize in the strong magnetic

field near a pulsar polar cap. These positrons can escape through magnetic fields that open through the light cylinder. The Lorentz factors of positrons made in this way are, however, usually so large that they will not thermalize on a time scale corresponding to the age of the Galaxy. The  $\gamma\gamma$  pair production process of the fifth row occurs in luminous compact regions that may be found in galactic black hole candidates, microquasars, active galactic nuclei, and in gamma-ray bursts (Dermer & Böttcher, these proceedings). Not listed in Table 1 are higher-order processes such as triplet pair production  $\gamma + e \rightarrow e^+ e^+ + e^-$ , and direct pair production  $e + N \rightarrow e + N + e^+ + e^-$ , which are generally much less important because of their small cross sections.

#### 3.1. Positron Production in Novae

There are four principal channels for the production of positrons in Novae; these are,

1.  $^{13}\text{Ni} \rightarrow ^{13}\text{C}$ ,  $\tau = 598$  s, 100%  $\beta^+$
2.  $^{18}\text{F} \rightarrow ^{18}\text{O}$ ,  $\tau = 109.8$  min, 96.9%  $\beta^+$
3.  $^{22}\text{Na} \rightarrow ^{22}\text{Ne}$ ,  $\tau = 2.60$  yr, 90.4%  $\beta^+$
4.  $^{26}\text{Al} \rightarrow ^{26}\text{Mg}$ ,  $\tau = 7.2 \times 10^5$  yr, 82%  $\beta^+$  and  $\gamma$ (1.809 MeV),

where we also list the half-life  $\tau$  and the fraction of decays that yield positrons. Nucleosynthesis in novae is discussed at this conference by Hernanz; here we only note that the first two channels of  $\beta^+$  production are sufficiently prompt that the produced positrons will annihilate in the dense material formed in the nova explosion Hernanz et al. (1999), whereas e $^+$  made through the latter two channels will be mixed in the expanding envelope and can be injected into the ISM. The Galaxy-averaged production rate of novae from Oxygen/Neon white dwarfs is estimated by (Hernanz et al., 1999a) to be  $\dot{N}_+^{22} \cong 5 \times 10^{39} - 2.4 \times 10^{40} \dot{N}_{\text{O}Ne/\text{yr}}$  e $^+$  s $^{-1}$  and  $\dot{N}_+^{26} \cong 7 \times 10^{38} - 4 \times 10^{40} \dot{N}_{\text{O}Ne/\text{yr}}$  e $^+$  s $^{-1}$  for the  $^{22}\text{Na}$  and  $^{26}\text{Al}$  channels, respectively. The quantity  $\dot{N}_{\text{O}Ne/\text{yr}}$  is the yearly rate of novae throughout the Galaxy. Starrfield et al. (1997) give  $\dot{N}_+^{22} \cong 8 \times 10^{38} - 5 \times 10^{40} \dot{N}_{\text{O}Ne/\text{yr}}$  e $^+$  s $^{-1}$  and  $\dot{N}_+^{26} \cong 6 \times 10^{39} - 2 \times 10^{41} \dot{N}_{\text{O}Ne/\text{yr}}$  e $^+$  s $^{-1}$  for these rates, which are slightly larger but consistent given the many uncertainties in the calculation. They also calculate the e $^+$  production rate from novae on CO white dwarfs, and obtain  $\dot{N}_+^{22} \cong 6 \times 10^{36} - 6 \times 10^{37} \dot{N}_{\text{CO}/\text{yr}}$  e $^+$  s $^{-1}$  and  $\dot{N}_+^{26} \cong 7 \times 10^{36} - 8 \times 10^{37} \dot{N}_{\text{CO}/\text{yr}}$  e $^+$  s $^{-1}$ . The yearly rate of novae throughout the Galaxy is estimated from observations to be  $\approx 35$  per year. If a significant fraction of these novae are produced on O/Ne white dwarfs, then novae can provide a non-negligible amount of the positrons injected into the Galaxy and would contribute to both the disk and bulge annihilation radiation.

### 3.2. Positron Production from SNe and Stellar Winds

The dominant channels for positron production and the associated  $\gamma$  ray lines formed through hydrostatic and explosive nucleosynthesis are

1.  $^{57}\text{Ni} \rightarrow ^{57}\text{Co}$ ,  $\tau = 36$  hr, 40%  $\beta^+$  and  $\gamma$ (1370 keV), followed by  $^{57}\text{Co} \rightarrow ^{57}\text{Fe}$ ,  $\tau = 271$  d,  $\gamma$ (122, 136 keV);
2.  $^{56}\text{Ni} \rightarrow ^{56}\text{Co}$ ,  $\tau = 6.1$  d,  $\gamma$ (150, 750, 812 keV), followed by  $^{56}\text{Co} \rightarrow ^{56}\text{Fe}$ ,  $\tau = 78.8$  d, 18%  $\beta^+$   $\gamma$ (847, 1238 keV);
3.  $^{44}\text{Ti} \rightarrow ^{44}\text{Sc}$ ,  $\tau \cong 62$  yr,  $\gamma$ (67.8, 78.4 keV), followed by  $^{44}\text{Sc} \rightarrow ^{44}\text{Ca}$ ,  $\tau = 3.93$  yr, 95%  $\beta^+$  and  $\gamma$ (1.16 MeV);
4.  $^{26}\text{Al} \rightarrow ^{26}\text{Mg}$ ,  $\tau = 7.2 \times 10^5$  yr, 82%  $\beta^+$  and  $\gamma$ (1.809 MeV).

The  $\beta^+$  decay lifetime from the channel 1 is too short to permit the positrons to escape from the ejecta into the ISM, so only a prompt 0.511 MeV line could be formed, and this would be severely degraded in optically thick material. The positron production rates into the ISM from Type Ia and Type II supernovae for the remaining channels depend sensitively on the percentage  $\eta_{-2}$  of positrons that escape into the ISM. For channel 2, Chan & Lingenfelter (1993) find that  $\dot{N}_+^{56,Ia} \cong 1.4 \times 10^{43} \eta_{-2} M_{56} \dot{N}_{Ia/C} \text{ e}^+ \text{ s}^{-1}$ , where  $M_{56}$  is the average number of solar masses of synthesized  $^{56}\text{Fe}$  per SN, and  $\dot{N}_{Ia/C}$  is the mean number of Type Ia SNe per century in the Milky Way. Woosley & Weaver (1992) calculate that  $0.6 < M_{56} < 0.9$ . From these rates, it is clear that Type Ia SNe are capable of making an important if not dominant contribution to positron production, depending crucially on the escape fraction  $\eta_{-2}$  (Milne et al., 1999a).

Positron production through the  $^{56}\text{Ni} \rightarrow ^{56}\text{Co} \rightarrow ^{56}\text{Fe}$  channel in Type II SNe is estimated by Chan & Lingenfelter (1993) to be  $\dot{N}_+^{56,II} \approx \times 10^{42} \eta_{-2} (M_{56}/0.08) \dot{N}_{II/C} \text{ e}^+ \text{ s}^{-1}$ . Because of the thickness of the overlying envelope in Type II SNe, the escape fraction is very poorly known and is probably  $\ll 1\%$ . At best, this channel could make a minor contribution to the total positron production rate in the Galaxy.

The much smaller synthesized mass of  $^{44}\text{Ti}$  compared with  $^{56}\text{Fe}$  means that the  $^{44}\text{Ti} \rightarrow ^{44}\text{Sc} \rightarrow ^{44}\text{Ca}$  channel makes a small contribution to the Galactic positron production rate from Type Ia SNe, even taking into account the longer decay time scale and larger positron escape fraction. The production rate from Type Ib and II SNe depends on the large uncertainties in the amount of synthesized mass per SNe. In the extreme case, the positron production rate from Type Ia, Ib, and II SNe is estimated to be  $\dot{N}_+^{44} \cong 10^{43} \text{ e}^+ \text{ s}^{-1}$  (Chan & Lingenfelter, 1993).

All positrons produced through the  $^{26}\text{Al} \rightarrow ^{26}\text{Mg}$  chain escape into the ISM due to the long lifetime of  $^{26}\text{Al}$ . The 1.809 MeV line therefore provides a tracer of positron production through channel 4. With an omnidirectional 1.809 MeV flux of  $\approx 3 \times 10^{-4} \text{ cm}^{-2} \text{ s}^{-1}$  (Diehl et al., 1995), this implies an associated Galactic positron production rate of  $\sim 2 \times 10^{42} \text{ e}^+ \text{ s}^{-1}$ . Type II SNe produce positrons from  $^{26}\text{Al}$  at a rate of  $\dot{N}_+^{26} \approx 10^{41} (M_{26}/10^{-5}) \dot{N}_{II/C} \text{ e}^+ \text{ s}^{-1}$ , where the mass of  $^{26}\text{Al}$  produced per SN ranges from  $0.3 \lesssim M_{26}/10^{-5} \lesssim 20$  (Prantzos, 1996). It is therefore likely that other sources contribute to  $^{26}\text{Al}$  production, such as massive stellar winds and novae. Winds from Wolf-Rayet stars produce positrons at the rate of  $\dot{N}_+^{26} \approx 1 \times 10^{42} \text{ e}^+ \text{ s}^{-1}$  (Meynet et al., 1997). AGB stars (Mowlavi, these proceedings) and novae can also make significant contributions. Thus the annihilation line map of the Galaxy should display a component that traces the 1.809 MeV map, although transport of the positrons from the production to the annihilation site could modify the spatial correlation, as would be the case for the positive latitude enhancement if due to a starburst/superwind (Dermer & Skibo, 1997).

### 3.3. Other Positron Sources

Cosmic rays produce positrons through the same strong interactions that produce  $\pi^0$  gamma rays. Thus the  $\pi^0$   $\gamma$ -ray emission centered at  $\approx 70$  MeV provides a tracer of positron production. COS-B analyses (Bloemen et al., 1984) imply that the Galaxy produces  $\sim 2.5 \times 10^{42} > 100$  MeV  $\text{ph s}^{-1}$ . The  $\pi^0$  and  $\pi^+$  production cross sections are roughly equal, though two  $\gamma$ -ray photons are made from each  $\pi^0$ . Thus the  $> 100$  MeV Galactic gamma-ray production rate also roughly represents an upper limit to the positron production rate from cosmic ray interactions, after correcting for the emission below 100 MeV and noting that bremsstrahlung and Compton photons substantially contribute to the diffuse Galactic gamma-ray background. Large fluxes of low-energy cosmic rays would also contribute to positron production through  $\beta^+$  decay of radioactive nuclei. COMPTEL upper limits to nuclear deexcitation gamma rays (Bloemen et al., 1999) suggest that positrons made through this process do not, however, significantly contribute to the overall Galactic annihilation line flux.

Although difficult to quantify, compact objects could eject large numbers of positrons into the ISM. Galactic black-hole candidate sources (Dermer & Liang, 1988) and microquasars (Li & Liang, 1996) are the two leading candidates for producing localized and time-variable sites of annihilation radiation. Individual sources could eject  $\sim 10^{41}\text{--}10^{42} \text{ e}^+ \text{ s}^{-1}$  into the ISM. Evidence has been presented from Sigma/Granat observations of 1E 1740.7-2942 and Nova Muscae for episodes of line emission at  $\approx 400$  keV that was attributed to redshifted annihilation radiation (for a review, see Harris, 1997), but OSSE

has not detected variable annihilation radiation or annihilation lines from black-hole candidate sources such as Cygnus X-1 (Philips et al., 1996). As already noted, electromagnetic cascades in pulsars would probably produce positrons with Lorentz factors too great to thermalize within the lifetime of the Galaxy. Production of positrons by GRBs in the Galaxy is discussed in a separate contribution (Dermer & Böttcher, these proceedings).

#### 4. POSITRON ANNIHILATION PROCESSES

Early calculations of positron annihilation in the ISM were treated by Bussard et al. (1979), and in Solar flares by Crannell et al. (1976). Updated cross sections and processes related to the annihilation of positrons are discussed in detail elsewhere (Gues-soum et al., 1991, 1997), so they are reviewed only briefly here. Positrons injected into the ISM will annihilate directly or thermalize. Thermalization is more important than annihilation for positrons injected at MeV energies, and direct annihilation of higher energy positrons produces a line that is invariably too broadened to be detectable. Positrons thermalize through Coulomb losses with free electrons, and through excitation and ionization energy losses with bound electrons. When a positron's energy reaches a few hundred eV, the energy-loss processes compete primarily with the formation of Ps through charge exchange in flight, as the rate of direct annihilation-in-flight is small. Thermal positrons either annihilate directly with free or bound electrons, or form Ps through radiative recombination and charge exchange. Charge exchange with neutral hydrogen has a 2430 Å threshold, so this process is suppressed in sufficiently low-temperature gases.

Ps is formed in the triplet ( ${}^3S_1$ ) ortho-Ps and singlet ( ${}^1S_0$ ) para-Ps ground states in a 3:1 ratio, with decay lifetimes of  $1.4 \times 10^{-7}$  s and  $1.25 \times 10^{-10}$  s, respectively. Cascading to the ground state can produce a Ly- $\alpha$  line at 6.8 eV and other lines that are very weak but, in principle, detectable (Burdyuzha & Kauts, 1994; Wallyn et al., 1996). Ps can be quenched if the density is  $\gtrsim 10^{13}$  cm $^{-3}$ , though this is not relevant for annihilation in the ISM. Annihilation of thermalized positrons on dust (Zurek, 1985; Gues-soum et al., 1991) is also an important quenching process for Ps, leading to a suppression of the  $3\gamma$  continuum. These calculations are complicated by grain properties, including their sizes, charges, and compositions. Guessoum et al. (1991) find that the presence of dust in the warm envelopes around cold molecular cloud cores can reduce the Ps fraction, but that dust is unlikely to affect the annihilation line and continuum properties in the uniform ISM.

Table 2. Binary interactions involving positrons.

| Energy Redistribution             | Positronium Formation           |
|-----------------------------------|---------------------------------|
| $e^+ H \rightarrow e^+ H^*$       | $e^+ e^- \rightarrow \gamma Ps$ |
| $e^+ H \rightarrow e^+ e^- H^+$   | $e^+ H \rightarrow H^+ Ps$      |
| $e^+ He \rightarrow e^+ He^*$     | $e^+ He \rightarrow He^+ Ps$    |
| $e^+ He \rightarrow e^+ e^- He^+$ |                                 |

| Positronium Quenching                | Annihilation                      |
|--------------------------------------|-----------------------------------|
| $e^- {}^3Ps \rightarrow e^- e^- e^+$ | $e^+ e^- \rightarrow 2\gamma$     |
| $H {}^3Ps \rightarrow H e^- e^+$     | $e^+ H \rightarrow H^+ 2\gamma$   |
| $e^- {}^3Ps \rightarrow e^- {}^1Ps$  | $e^+ He \rightarrow He^+ 2\gamma$ |
| $H {}^3Ps \rightarrow H {}^1Ps$      | ${}^1Ps \rightarrow 2\gamma$      |
| $H^+ Ps \rightarrow H e^+$           | ${}^3Ps \rightarrow 3\gamma$      |
| $He^+ Ps \rightarrow He e^+$         |                                   |

#### 5. CALCULATIONS OF ANNIHILATION LINE AND CONTINUUM SPECTRA

We have developed a computer code to calculate the 0.511 MeV line spectrum and relative strength of the  $3\gamma$  continuum. The code incorporates updated cross sections to calculate thermally-averaged rates for all relevant binary interactions involving positrons, and uses a Monte Carlo technique to simulate the thermalization and Ps production of  $\sim$ MeV positrons. We include charge exchange with neutral and singly-ionized helium, which have generally been ignored in astrophysical applications. Processes involving dust and  $H_2$  are not yet included.

For the formation of Ps, we include radiative recombination with free electrons and charge exchange with hydrogen and neutral He. For Ps quenching, we include breakup of Ps by neutral hydrogen, ortho-Ps quenching via free electrons and via electrons bound in H, inverse charge exchange with H and He, and ionization of ortho-Ps atom by free electrons. This last reaction turns out only to be important in ionized gases at densities  $\gtrsim 10^{13}$  cm $^{-3}$ , and is relevant to positron annihilation at the Sun.

For the Monte Carlo determination of the fraction of positrons forming Ps before thermalization and the resulting Ps energy distribution, we include He and we use an updated experimentally-determined cross section for charge exchange in hydrogen. We find that this new cross section results in higher Ps production than previously calculated, and the resulting annihilation line width is broader.

The Ps formation, quenching and energy loss processes along with the positron annihilation processes treated in our calculations are shown in Table 2. The important diagnostic spectral features of annihilation radiation are the ratio  $Q_{3\gamma}/Q_{2\gamma}$  and the FWHM width  $\Delta E$  of the line. These two quantities depend

Table 3. Temperatures and densities, in units of  $\text{cm}^{-3}$ , of different phases of the ISM used in calculations of annihilation radiation

|                    | Cold<br>Neutral | Warm<br>Neutral | Warm<br>Ionized | Hot                  |
|--------------------|-----------------|-----------------|-----------------|----------------------|
| T(K)               | 80              | 8000            | 8000            | $4.5 \times 10^5$    |
| $n_{\text{HI}}$    | 38              | 0.31            | 0.06            | 0.0                  |
| $n_e$              | 0.0             | 0.055           | 0.17            | $3.5 \times 10^{-3}$ |
| $n_{\text{HII}}$   | 0.0             | 0.055           | 0.17            | $2.9 \times 10^{-3}$ |
| $n_{\text{HeI}}$   | 3.8             | 0.036           | 0.023           | 0.0                  |
| $n_{\text{HeII}}$  | 0.0             | 0.0             | 0.0             | 0.0                  |
| $n_{\text{HeIII}}$ | 0.0             | 0.0             | 0.0             | $0.6 \times 10^{-3}$ |

upon the conditions of the medium where the annihilation occurs. The medium can be characterized by the temperature  $T$ , the total (neutral + ionized) hydrogen density  $n_H$ , and the ionization fractions  $X_{H^+}$ ,  $X_{He^+}$  and  $X_{He^{++}}$ . We use the non-thermal and thermally-averaged rates discussed above to solve a system of continuity equations for pair equilibrium and provide rates for positron annihilation from all of the various processes. These rates then directly give  $Q_{3\gamma}/Q_{2\gamma}$ . The total line spectrum is the sum of several components, some having Gaussian shapes, others not. Hence, the total line shape will not, in general, be Gaussian.

Fig. 2 shows calculations of the annihilation line and Ps continuum for phases of the ISM with temperatures and densities given by Table 3. Fig. 3 shows calculations of the same quantities for high temperature, fully ionized media. The quantities  $Q_{3\gamma}/Q_{2\gamma}$ , giving the relative number of photons in the  $3\gamma$  Ps continuum to the 0.511 MeV line, and the FWHM line width  $\Delta E$ , from Figs. 2 and 3, are plotted in Fig. 4. In the limit of a fully neutral medium, all annihilation takes place through the formation of Ps. Consequently  $Q_{3\gamma}/Q_{2\gamma} \rightarrow 9/2$ , because 3/4 of the annihilations take place via ortho-Ps, giving 3 photons per annihilation, whereas 1/4 of the annihilations take place via para-Ps, giving 2 photons per annihilation. Annihilation occurs before thermalization in a fully neutral medium, so the calculated 9 keV line width for the neutral medium is broader than for partially ionized media where the positrons generally thermalize before annihilating.

As the temperature increases, the relative number of  $3\gamma$  continuum to  $2\gamma$  line photons decreases. This is because the Ps formation processes involving charge exchange with neutrals become less important at higher temperatures due to the fewer available neutral or partially ionized ions. The line width increases at high temperatures due to thermal broadening, and approaches the limit  $\Delta E_{\text{FWHM}} = 11.0T_6^{1/2}$  keV (Crannell et al., 1976; Guessoum et al., 1997), where  $T_6$  is the temperature in units of  $10^6$  K.

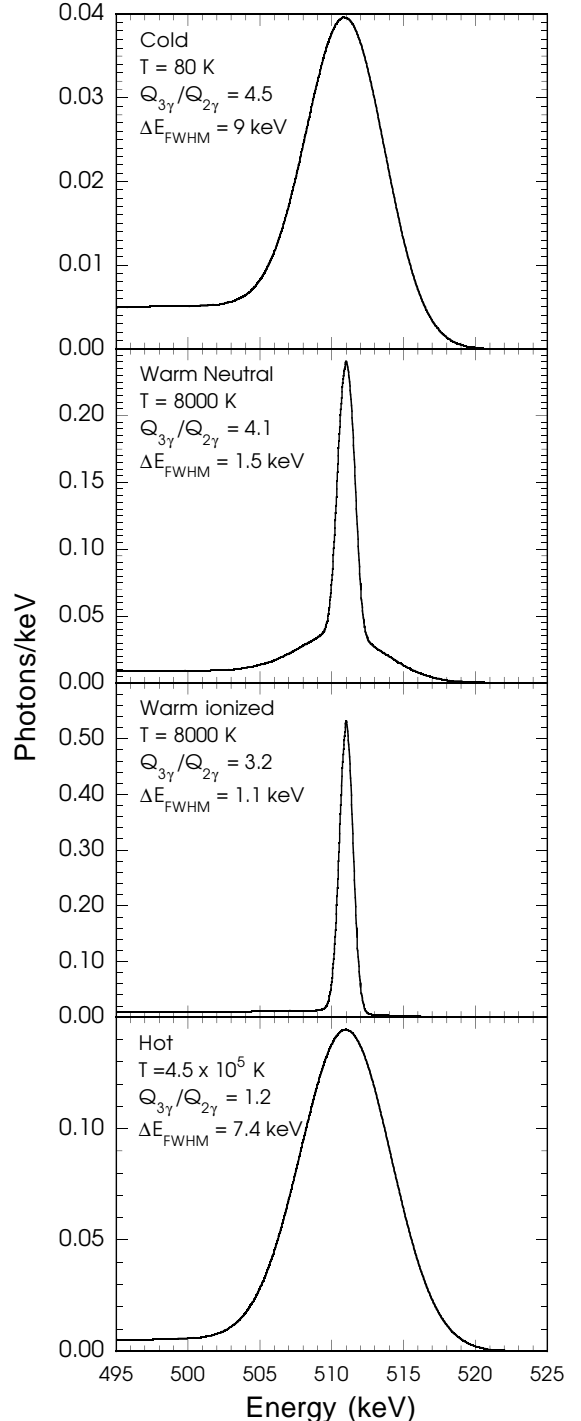


Figure 2. Calculations of annihilation line and Ps continuum from the injection of MeV positrons into regions with different temperatures and ionization fractions.

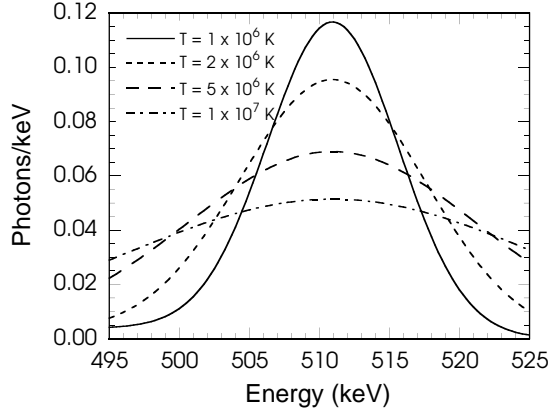


Figure 3. Calculations of annihilation line and  $Ps$  continuum from the injection of MeV positrons into high temperature plasma.

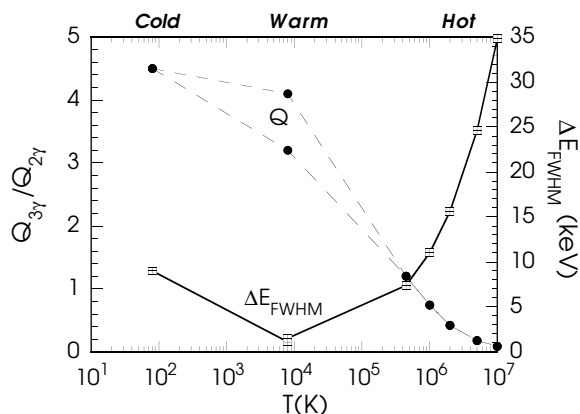


Figure 4. Calculations of  $3\gamma/2\gamma$  ratios and FWHM line widths in different phases of the ISM.

Fig. 4 quantitatively shows how the  $3\gamma$   $Ps$  continuum is quenched in high temperature plasmas. Consequently  $Ps$  formation can be quenched in high temperature gas. This property can account for the marginal detection or absence of a high-latitude enhancement in the  $Ps$  maps of the Galactic Center region as compared with the observation of a high-latitude enhancement in the 0.511 MeV line maps (Milne et al., 1999). If this interpretation is correct, then a broadened annihilation line would be detected in the direction of the high-latitude enhancement with a line width  $\Delta E_{FWHM} \gtrsim 10$  keV and with an intensity  $\sim 1.2 \times 10^{-4}$  ph cm $^{-2}$  s $^{-1}$ . For broad FoV instruments such as TGRS (Harris et al., 1998), this broadened line is difficult to resolve from the narrow, bright annihilation line emitted by the disk and bulge components. The imaging capability of *INTEGRAL* will be able to determine whether the interpretation of the high latitude enhancement as a fountain of hot gas venting into the halo of the Galaxy is correct by mapping the intensity and line width in this direction, provided that the positive latitude enhancement is sufficiently localized. Further work will be required to determine if  $Ps$  can be quenched by dust in the Galactic Center region, which could also lead to suppression of the  $3\gamma$   $Ps$  continuum.

## 6. SUMMARY AND CONCLUSIONS

We have summarized our knowledge of astronomical sources of positrons and the processes that lead to the formation of annihilation radiation in the ISM. Because of the large uncertainties in nucleosynthesis calculations, the relative contributions of novae, SNe, and Wolf-Rayet winds remains unclear. Positrons from cosmic rays, compact objects, and GRBs could also make a significant contribution to positron production in the Galaxy. An important tool to reveal the dominant sources of positrons will be to use  $\gamma$ -ray tracers to establish associated positron injection rates. COMPTEL and *INTEGRAL* maps of the  $^{26}\text{Al}$  1.809 line and EGRET maps of  $\pi^0$  gamma-ray emission should trace some fraction of the annihilation glow of the Galaxy, with the residual attributed to other processes.

One of the lingering uncertainties in positron astrophysics is the question of whether positrons are formed by accreting compact objects in the Galaxy. SPI on *INTEGRAL* will be well suited to examine this question, not only by searching for annihilation line transients, but also by looking for annihilation hot spots that are coincident with compact object emission in the Galaxy. SPI's 511 keV sensitivity for on-axis point sources during a  $10^6$  s observation is  $2.3 \times 10^{-5}$  ph cm $^{-2}$  s $^{-1}$  (Vedrenne et al., 1999). Spectral analysis may show that annihilation photons from directions coincident with known compact objects have a different line width or  $3\gamma/2\gamma$  ratio than the surrounding emission, suggesting a point source origin. For sufficiently bright sources, SPI could provide sub-degree imaging that could be com-

pared with IBIS maps of point sources. Searches for variations of the Ps fraction and line width will reveal if there are unusual sites of positron production, and whether the emission from the positive latitude enhancement arises from annihilation in a hot superwind or at compact objects.

#### ACKNOWLEDGMENTS

This work is supported by the Office of Naval Research. We thank P. A. Milne and M. J. Harris for discussions.

#### REFERENCES

Bloemen, J.B.G.M., Blitz, L., Hermsen, W., 1984, *ApJ*, 279, 136

Bloemen, H., et al., 1999, *ApJ*, 521, L137

Bussard, R.W., Ramaty, R., Drachman, R.J., 1979, *ApJ*, 228, 928

Burdyuzha, V.V., Kauts, V.L., 1994, *ApJS*, 92, 549

Chan, K.W., Lingenfelter, R.E., 1993, *ApJ*, 405, 614

Cheng, L.X., et al., 1997, *ApJ*, 481, L43

Crannell, C.J., Joyce, G., Ramaty, R., Werntz, C., 1976, *ApJ*, 210, 582

Dermer, C.D., Skibo, J.G., 1997, *ApJ*, 487, L57

Dermer, C.D., and Liang, E.P., 1988, in *Nuclear Spectroscopy of Astrophysical Sources*, ed. N. Gehrels and G.H. Share (New York: AIP), 326

Diehl, R., et al., 1995, *A&A*, 298, 445

Guessoum, N., Ramaty, R., Lingenfelter, R.E., 1991, *ApJ*, 378, 170

Guessoum, N., Skibo, J.G., Ramaty, R., 1997, in the *Second INTEGRAL Workshop*, ed. C. Winkler, T. Courvoisier, Ph. Durouchoux (ESA SP-382), 113

Harris, M.J., Teegarden, B.J., Cline, T.L., Gehrels, N., Palmer, D.M., Ramaty, R., Seifert, H., 1998, *ApJ*, 501, L55

Harris, M.J., 1997, in the *Fourth Compton Symposium*, ed. C.D. Dermer, M.S. Strickman, and J.D. Kurfess (New York: AIP), 418

Harris, M.J., Share, G.H., Leising, M.D., Kinzer, R.L., Messina, D.C., 1990, *ApJ*, 362, 135

Hernanz, M., José, J., Coc, A., Gómez-Gomar, J., Isern, J., 1999, *ApJ*, 526, L97

Hernanz, M., José, J., Coc, A., Gómez-Gomar, J., Isern, J., 1999, in the *Fifth Compton Symposium*, ed. M. L. McConnell and J. M. Ryan (New York: AIP), 97

Johnson, W.N., Haymes, R.C., 1973, *ApJ*, 184, 103

Kinzer, R.L., Purcell, W.R., Kurfess, J.D., 1999, *ApJ*, 515, 215

Leventhal, M., MacCallum, C.J., Stang, P.D., 1978, *ApJ*, 225, L11

Li, H., Liang, E.P., 1996, *ApJ*, 458, 514

Lingenfelter, R.E., Ramaty, R., 1989, *ApJ*, 343, 686

Mahoney, W.A., Ling, J.C., Wheaton, W.A., 1994, *ApJS*, 92, 387

Meynet, G., Arnould, M., Prantzos, N., Paulus, G., 1997, *A&A*, 320, 460

Milne, P.A., Kurfess, J.D., Kinzer, R.L., Leising, M.D., Dixon, D.D., 1999, in the *Fifth Compton Symposium*, ed. M.L. McConnell and J.M. Ryan (New York: AIP), 21

Milne, P.A., The, L.S., Leising, M.D., 1994, *ApJS*, 124, 504

Phlips, B.F., et al., 1997, *ApJ*, 465, 907

Prantzos, N., 1996, *A&AS*, 120, 303

Purcell, W.R., et al., 1997, *ApJ*, 491, 725

Ramaty, R., Skibo, J.G., Lingenfelter, R.E., 1994, *ApJS*, 92, 393

Skibo, J.G., 1993, PhD Thesis, Univ. of Maryland

Share, G.H., Leising, M.D., Messina, D.C., Purcell, W.R., 1990, *ApJ*, 358, L45

Share, G.H., et al., 1988, *ApJ*, 326, 717

Starrfield, S., Truran, J.W., Wiescher, M.C., Sparks, W.M., 1997, in the *Fourth Compton Symposium*, ed. C.D. Dermer, M.S. Strickman, and J.D. Kurfess (New York: AIP), 1130

Vedrenne, G., et al., 1999, *Astron. Lett. and Communications*, 39, 325

Wallyn, P., Mahoney, W.A., Durouchoux, P., Chappuis, C., 1996, *ApJ*, 465, 473

Woosley, S.E., Weaver, T.A., 1992, in *Supernovae*, ed. J. Audouze et al. (New York: Elsevier)

Zurek, W.H., 1985, *ApJ*, 289, 603